HMT-2019-716
Revised manuscript

Color code:

Revisions in response to recommendations from Referee 1

Revisions in response to recommendations from Referee 2

Revisions in response to recommendations from Referee 3

A small scale experiment and a simplified model to investigate the runaway of sodium-water reaction

Lucas David[a,b,*], François Beauchamp[a], Alexandre Allou[a], Richard Saurel[b], Paul Guiffard[a], and Kevin Daudin[a]

[a]CEA, DEN, DTN/STCP/LTPS, Cadarache, F-13108 Saint-Paul-lez-Durance, France
[b]LMA, CNRS UMR 7031, Centrale Marseille, F-13402 Marseille cedex 20, France
[*]Corresponding author. Email : lucas.david@cea.fr Tel : +33 6 68 72 68 29

July 18, 2019

Abstract

Sodium-Water Reaction (SWR) is a notorious and complex interaction between two condensed phase reactants. It involves both physical and chemical processes, is fast, exothermic, and can be explosive under specific conditions. The fine-scale processes of SWR, and in particular the runaway mechanism eventually leading to explosive effects, are not yet fully understood. This paper focuses on how SWR runaway is triggered. Experiments investigating the processes of SWR with a high-speed camera are first described. These experiments suggest that sodium vaporization is responsible for provoking runaway. The main experimental observations are discussed and a scenario for SWR runaway is proposed. Finally, a semi-analytical model based on that mechanism is developed. Physical considerations and simplifying assumptions allow reducing the model to a single differential equation in the configuration of current experiments. The results of this model are consistent with experimental observations, and confirm the critical role of sodium vaporization in the onset of SWR runaway.

Keywords: sodium-water reaction, runaway, experiment, high-speed camera, modeling

1 Introduction

Sodium is an alkali metal used in liquid state as a coolant for Sodium Fast-neutron Reactors (SFR). SFR is of great industrial interest for power generation because it offers improved nuclear fuel utilization, high energy conversion efficiency and a potential solution for the treatment of certain long-lived nuclear waste. However its operation requires the control of the risks associated to the chemical reactivity of sodium, such as sodium-water reaction (SWR).

SWR is a vigorous exothermic reaction generating hydrogen and sodium hydroxide:

$$\mathrm{Na} + \mathrm{H_2O} \longrightarrow \mathrm{NaOH} + \frac{1}{2}\,\mathrm{H_2} \tag{1}$$

In the context of SFR, SWR is mainly studied in the incidental scenario of heat exchanger tube failure in a steam generator [1–4]. In such situation, pressurized water in liquid and vapor forms leaks into the sodium circuit and causes SWR which can result in serious steam generator damage. SWR can also occur in another configuration for which research is less advanced: the case of uncontrolled water entry during maintenance operations (*e.g.,* cleaning of sodium-wetted reactor components or spent fuel assemblies) or during SFR dismantling. In such a configuration, the reaction mode is very different from that of steam generators, because SWR occurs with initially solid sodium in excess liquid water, instead of water vapor in excess liquid sodium.

To improve the prevention and management of these risks, it is important to have a good understanding of the physics of the sodium-water reaction. The purpose of the present work is to advance the knowledge of a fundamental aspect of SWR: the occurrence of explosive effects in the configuration of initially solid or liquid sodium in excess water.

The potentially explosive behavior of SWR is a widely known phenomenon, often demonstrated as an example of the high reactivity of alkali metals. However the process leading to SWR explosions has not yet been fully explained nor modeled, and keeps being investigated.

Not long ago, the explosions were attributed to the spontaneous combustion of the dihydrogen gas produced by SWR with air [5]. But Carnevali et al. [6] recently examined SWR in an inert atmosphere, thus preventing the combustion of hydrogen. They clearly observed blast waves, showing SWR alone can cause explosions. Observing that no explosion occurred if the sodium sample was placed on a heat sink made of copper, they also put in evidence that sodium heating was a key element in the explosive process [7].

Daudin et al. [8] then used a high-speed camera along with pressure and temperature sensors to further investigate SWR. They observed that the phenomenology, in particular the occurence of explosive effects, was dependent on the temperature of the reactants and on their mixing mode. When explosions occured, they did not happen immediately but a short delay after contact of the reagents. Also, less than 10% of the available chemical energy given by reaction (1) (considered total and instantaneous) was recovered as mechanical energy in the blast wave. They finally noted that a gas

film appeared between sodium and water which seemed to have a major role in the interaction. This gas film had also been observed earlier by Ashworth [9]. However, the large scale of Daudin's experiment and the dispersion of the results were a limit to making further observations on the fine-scale processes involved.

Mason et al. [10] were able to closely observe the first instants of SWR at very small scale (about 100 mg of metal with liquid water in excess). They identified a Coulomb explosion, due to electronic repulsion between ionized alkali atoms, leading to the rapid increase of the reactants contact surface and consequently of the reaction rate, which they were able to confirm with *ab initio* molecular dynamics computations. At larger scales, this description is however restricted to the first milliseconds following the contact. As reactants get rapidly separated by a gas film, other phenomena occur and a different description becomes necessary. Finally Marfaing et al. [11] proposed a low Mach number model of the gaseous film, which described SWR as a diffusion flame. They showed in particular that the sodium hydroxide produced by SWR was mainly in form of aerosol rather than gas, but still did not explain the explosive behavior of SWR.

In order to deeper understand the mechanism of explosion onset during SWR, a small-scale experiment called VIPERE has been carried out. Novel observations have been made thanks to close up high-speed photography, which led to observe that sodium boiling may be responsible for triggering explosions. This paper is organized as follows. Section 2 presents VIPERE experiments and the discussion that led to the formulation of this new SWR scenario. In Section 3, a reduced mechanistic model based on a single differential equation to describe SWR processes is proposed. Its results are compared to the postulated phenomenology and experimental observations.

2 VIPERE experiments

2.1 Experimental setup and procedure

The goal of VIPERE experiments is to provide reproducible small-scale observations of SWR with a simple setup (Fig. 1). For each test, a 1 g spherical solid sodium sample is prepared under inert atmosphere in a glove box at ambient temperature. A water volume of 2.5 L, contained in a ⌀16 cm pyrex beaker, is heated at a given temperature. Sodium is flushed by argon gas towards liquid water through a flexible tube. The atmosphere around the reaction zone is also kept inert by a continuous argon flow. The reaction is then recorded using a Phantom high-speed camera (model v411 for tests 1 to 34 and v1612 for tests 35 to 43) and a led panel is used for backlighting. Camera speed ranges from 8 000 to 130 000 fps. Pressure signals are recorded in air by 2 piezoelectric sensors P1 and P2 (amplitude 7 bar, frequency 150 kHz) located respectively 55 and 60 cm above the water surface. The only variable parameter is the water temperature, in the range [10-99 °C]. 43 tests have been carried out.

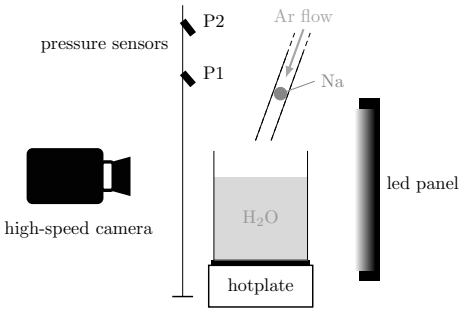

Figure 1: Schematic representation of VIPERE experimental setup. A 1 g spherical solid sodium pellet is put in contact with liquid water. The reaction is filmed using a high-speed camera.

2.2 General observations

The formation of gas is observed as soon as the sodium sample penetrates water. This gas is H_2 formed by SWR, with possibly some argon dragged from the surface. The gas appears first as millimeter size bubbles (Fig. 2a). Bubbles rapidly coalesce to form a gas film all around the sample. Large gas pockets form on top of the sample and periodically detach to reach the surface (Fig. 2b). As sodium is lighter than water, it rapidly goes up to the surface that it reaches about 400 ms after contact.

At the surface, the sodium stabilizes on a thin gas layer (Fig. 2c). It fastly spins and randomly moves on the surface. The thickness of the gas layer is nearly constant (about 1 mm). As seen from deformations of the pellet in the videos, the sodium becomes liquid shortly after the beginning of the reaction. This stage is reminiscent of the Leidenfrost effect in which a liquid drop floats without friction on its own vapor, except it is chemically driven instead of thermally. The white coloration characteristic of hydrated sodium hydroxide is observed in the water (Fig. 2d) and eventually at the sodium surface (Fig. 2e). For certain tests at especially low water temperature ($T_{H_2O} \leq 27\,°C$), the sodium is entirely consumed at this stage and no explosion occurs or only a small burst.

But in most cases, after a hundred milliseconds to a few seconds in the Leidenfrost-like stage, a sudden energy release is observed. It is characterized by the emission of a stiff pressure wave (recorder in air by two pressure sensors) and the expansion of the gas film repulsing liquid water away. The velocity of the gas front ranges from 7 to 30 $m\,s^{-1}$ depending on the energy of the blast. Explosions, which generate a blast wave (Fig. 5), are systematically accompanied by an orange-yellow luminous flash which appears locally and promptly extends to the whole gas layer, at a typical speed of 500 $m\,s^{-1}$ (Figs. 2f, 2g, 3). Reciprocally, no blast wave is recorded when flash is absent. For high water temperatures ($T_{H_2O} \geq 78\,°C$), explosions often occur underwater, very rapidly after reactant contact, and are less intense. The case of underwater explosions also occurred exceptionally for intermediate (50-60 °C) water temperatures. An expulsion of unreacted liquid sodium in the air is also visible on most tests (Fig. 2h), particularly for weak explosions. This remaining sodium often breaks up in smaller parts which react when falling back into water, though with a lower intensity. The time between contact of the reactants and runaway, called delay time, is found to be decreasing with water

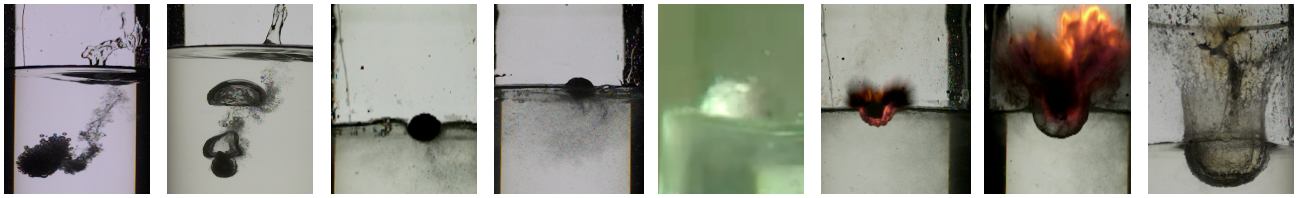

(a) Gas bubbles form immediately after penetration

(b) Bubbles coalesce in a film and gas pockets detach

(c) Sodium floats and spins on a gas layer

(d) NaOH dissolution forms a whitish trail

(e) Liquid NaOH produced at the surface of the sodium pellet

(f) Ignition flash preceding explosive effects

(g) Intense explosions induce luminescence

(h) Unreacted liquid sodium is ejected

Figure 2: General observations made during reactions following the impact and penetration of 1 g sodium pellets in liquid water. The phenomenology depends on water temperature as discussed in Section 2.2.

Figure 3: Apparition and propagation of an ignition flash ($T_{H2O} = 52\,°C$). Ignition appears locally and promptly extends to the whole gas film.

temperature (Fig. 10). It is measured using video recordings.

2.3 Observations on the explosion onset

On several high speed videos, a dark steam is observed emanating from the sodium sample. This steam, which is possibly sodium vapor, appears in the instants preceding the explosion (40 to 400 ms before), and is also visible in the expanding bubble afterwards (Fig. 4). The apparition of this steam seems closely related to the onset of the explosion, and suggests that sodium vaporization may be responsible for provoking runaway.

2.4 Pressure signals

For low water temperatures ($T_{H_2O} \leq 27\,°C$), no explosive event is observed (only puffing eventually), and pressure sensors do not detect any pressure variation. For intermediate temperatures ($27\,°C \leq T_{H_2O} < 78\,°C$), violent runaways give rise to stiff pressure waves, with typical profiles of blast waves. These signals typically feature 30-40 mbar peak pressure with a rise time about of 20 µs, and a propagation velocity of about $280\,m\,s^{-1}$. Last, for higher water temperatures ($T_{H_2O} \geq 78\,°C$), explosions occur while sodium is still underwater. Pressure signals recorded are then harder to characterize as waves cross several interfaces before reaching the transducers. A first pressure peak (a few mbar) is detected, followed by a pressure drop due to release of hot gases and bubble collapse. Water

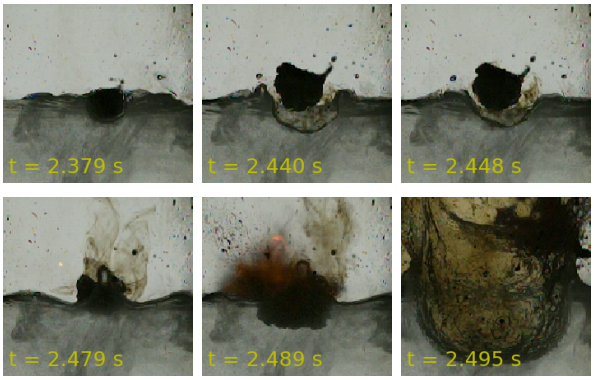

Figure 4: Apparition of a dark steam emanating from sodium in the instants preceding ignition (test 11, $T_{H_2O} = 53\,°C$).

projections on the sensors also bring variation to the signal. Typical examples of these three cases are displayed on Fig. 5.

2.5 Discussion

2.5.1 On the nature of the fume observed

Considering the species present in Equation (1), there are 4 options for the nature of the fume observed in Section 2.3 : water vapor, hydrogen, sodium vapor or sodium hydroxide aerosol. Sodium vapor has a "dark violet" color at high density [12], and can appear only after sodium is hot enough to start evaporating. It is therefore a plausible solution as the fume is noticed only at a late stage of the reaction. It is also consistent with the recent observations of Mason et al. [13], who identified sodium and potassium vapors in a late stage of the reaction of a NaK drop with water using a spectrometer, and estimated the drop temperature to be about 600 °C at that moment, which is close to NaK boiling temperature (785 °C). The 3 other species on the other hand are present from the beginning of the reaction, and should thus be noticed from the start if they constitute that fume. Hydrogen is ruled for being invisible.

2.5.2 On the origin of the luminescence

Orange and yellow light is emitted from the reaction zone during ignition and explosion (see Figs. 3 and 2g). This luminescence may also be attributed to sodium vapor which is thermoluminescent, especially as the other species present are not emissive. $OH^\bullet$ chemiluminescence was also considered ($OH^\bullet$ is present as a short-lived intermediary radical), but it emits in the ultraviolet range (313 nm wavelength) whereas the observed light is visible. At low vapor pressure, sodium emits quasi-monochromatic yellow light, due to its doublet at 589 nm. This doublet is responsible for the characteristic yellow light emitted by low-pressure sodium (LPS) lamps. At higher vapor pressures (20-120 kPa), the Na(v) emission spectrum broadens and most of the intensity is located in the 600-800 nm (orange-red) region [14].

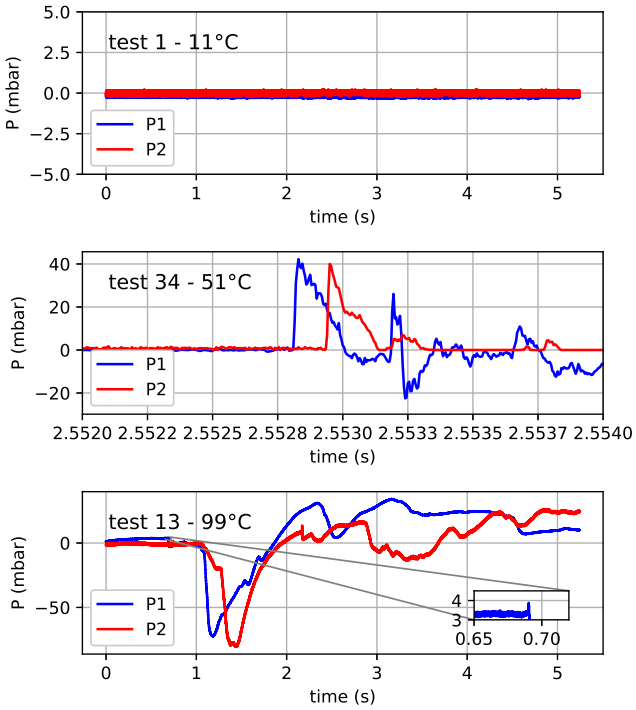

Figure 5: Three different types of typical pressure signals recorded during VIPERE experiments. The two sensors P1 and P2 are distant of 5 cm. Blast waves are recorded for intermediate water temperatures ($27\,^{\circ}\mathrm{C} < T_{\mathrm{H_2O}} \leq 78\,^{\circ}\mathrm{C}$). For lower temperatures, no pressure variation is recorded. For higher temperatures, weak explosions occur underwater and signals are damped. Only a small peak is detected followed by a depression due to the expansion of hot gases and to bubble collapse.

The orange and yellow colors visible on Fig. 2g could thus be both due to Na(v) thermoluminescence. The halo is orange-red at the vicinity the fragmented liquid sodium and yellow at its periphery, which would be coherent with the fact that the orange color corresponds to a higher sodium vapor pressure.

2.5.3 On the explosion type

The phenomenology observed in VIPERE experiments is reminiscent of several characteristic explosion types. The existence of a delay time before explosion shows that SWR is clearly a runaway reaction in that configuration.

As the presence of an explosion and the duration of the delay time depend on water temperature (Fig. 10), this runaway must be a thermal process. The theory of thermal runaways (or thermal explosions) has been developed by Semenov [15] and Kamenetskii [16]. These processes are governed by an energetic balance between heat production and loss, and chemical kinetics dependent on temperature through Arrhenius law. When the reactants reach a sufficient temperature, the kinetics become fast enough for heat production to be greater than losses, and the system diverges (explosion). This kind of model is similar to SWR by many aspects, however it is valid only for reactions with premixed reactants and chemical kinetics as a limiting step. This is not the case of SWR that has a low activation energy [17] and separated reactants.

SWR is also reminiscent of vapor explosions, provoked by the contact of a hot metal with a cold liquid refrigerant [18]. This contact generates a vapor film that isolates the metal from the refrigerant. After some delay time, an hydrodynamic instability may lead to a contact between the metal and the refrigerant (film collapse). A violent heat transfer would then vaporize much of the refrigerant and cause fragmentation of the metal, creating more contact surface and vapor generation. The expansion of the abruptly produced steam constitutes an explosion. SWR is similar to vapor explosions for its gas film, its delay time and the stiff generation of vapor. But its gas film is mostly constituted of a gas produced by the reaction (H_2) rather than vapor, and no direct film collapse has been observed to cause ignition during VIPERE experiments.

Finally, SWR has several common features with droplet micro-explosions. These explosions are commonly observed during combustion of hydrocarbon fuel droplets [19]. They are caused, after a delay time, by nucleation and violent boiling inside the fuel droplet, that leads to its fragmentation. Sodium also seems to boil before ignition during SWR. But micro-explosions are observed at a much smaller scale ($\sim 1\,\mathrm{mg}$ fuel droplets), and with a gaseous oxidizer, whereas in this configuration SWR features a pure fuel and a liquid oxidizer.

In spite of the similarities observed, SWR cannot be classified in any of the explosion categories cited above. It therefore seems that SWR has its very own process, which is a combination of all of them.

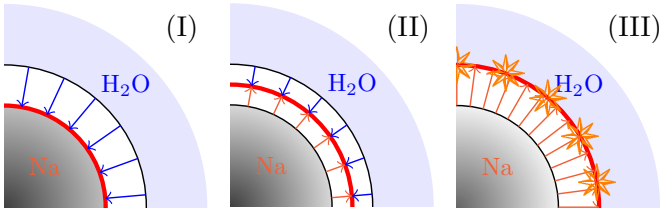

Figure 6: From left to right, the three step of the phenomenology postulated for SWR : (I) surface reaction, (II) gas-phase reaction, (III) runaway. The red surface symbolizes the reaction zone. The distinction between surface and gas-phase reactions during SWR was also made by Takata et al. [17].

2.5.4 Postulated phenomenology

Considering all the observations and analysis reported in this section, *we postulate that SWR runaway is triggered by sodium vaporization.* This hypothesis is further supported by the following considerations:

- The limiting step of SWR is the supplying of reactants through the gaseous film. This limiting step disappears when sodium vapor invades the film and meets the gas-water interface;
- Sodium vapor saturation pressure is an exponential function of temperature [20]. This exponential behavior is a likely cause of the thermal runaway (such as the Arrhenius law in thermal explosions models);
- Because of its very high thermal diffusivity, sodium acts as a heat sink and absorbs energy to heat up. But when it approaches boiling temperature, all the energy transferred serves to produce vapor which feeds the reaction and its runaway.

We believe that SWR proceeds in 3 steps: surface reaction (I), gas-phase reaction (II), and runaway (III), as sketched on Fig. 6. A gas film immediately forms between reactants after they are put in contact. Water vapor then diffuses through that film and reacts with sodium at the surface of the pellet (surface reaction step). The energy released heats the sodium. When sodium becomes hot enough (from 300-400 °C), it starts producing vapor as well. This vapor diffuses in the film until it meets water vapor to react (gas-phase reaction step). A diffusion flame sets in the film [11]. As sodium temperature keeps increasing, its vapor pressure and evaporation rate rise too, and the reaction front moves towards the gas-water interface. Eventually, sodium approaches boiling temperature and absorbs less power, until the heat generated becomes too high to be absorbed or dissipated, inducing runaway.

3 Semi-analytic differential model

In this section, a mechanistic model based on the phenomenology described in Section 2.5 is proposed. This model describes the reaction between a 1 g sodium spherical sample and liquid water in excess. This configuration is similar to that of VIPERE experiments. The model takes one input variable T_{H_2O} and one parameter D, which is the diffusion coefficient of sodium and water vapors in the gas layer, and that governs the kinetics of the process. It is built after a detailed analysis of orders of magnitude and time scales, used to draw several simplifying assumptions. These are presented in Section 3.1. In Section 3.2, the equations of the model and their resolution are detailed. Finally in Section 3.4, results are presented, compared to the experimental data and discussed.

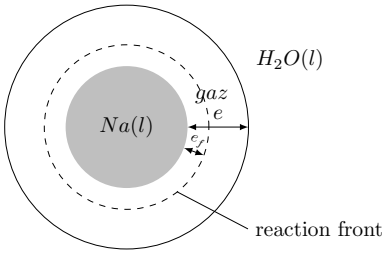

Figure 7: Configuration studied for the construction of the model. Sodium sample diameter is about 1 cm and film thickness e is about 1 mm.

3.1 Physical considerations and simplifying hypothesis

We consider a spherical sodium sample with a mass of 1 g (diameter$\sim$ 1.3 cm) separated from water by a gas film of thickness e (Fig.7).

3.1.1 Temperature variations

Average thermal properties of sodium and water, recalled in Table 1, show that sodium is nearly 500 times more diffusive than water. This means that water temperature variations are negligible compared to those of sodium. Water temperature is therefore assumed to remain constant during a given experiment, especially as it is in large excess.

Furthermore, sodium's high diffusivity tends to flatten the temperature profile in the sample. Considering also its small size, weak temperature gradients are expected between the center and the surface of the ball. This was checked by numerical resolution of the heat equation in one-dimension with spherical symmetry. In the configuration of the present model, sodium temperature is therefore considered uniform.

Table 1: Thermal properties of sodium [20] and water. Properties have been averaged over [0-883 °C] for sodium and [0-100 °C] for water.

	sodium	water
conductivity λ ($\mathrm{W\,m^{-1}\,K^{-1}}$)	75	0.62
density ρ ($\mathrm{kg\,m^{-3}}$)	850	990
heat capacity c_p ($\mathrm{J\,kg^{-1}\,K^{-1}}$)	1300	4000
diffusivity $D = \frac{\lambda}{\rho c_p}$ ($\mathrm{m^2\,s^{-1}}$)	6.9×10^{-5}	1.6×10^{-7}

3.1.2 Modeling of the chemical reaction

As postulated in Section 2.5, the reaction occurs successively at the sodium surface and in the gas phase [17]. We propose here a single description that covers both forms.

- **Location.** We suppose that the reaction takes place at a front distant of e_f from the sodium surface (Fig. 7). If $e_f \approx 0$ it corresponds to a surface reaction, and if $e_f > 0$ to a gas phase reaction.

- **Energy.** We consider the net energy balance of SWR, that is to say the heat released by the reaction reduced by the latent heat of vaporization of the gaseous reactant(s). This way, it appears that the energy balance is the same for surface and gas-phase reactions. Indeed, the difference between the energy generated by the gas-phase reaction $Q_{\mathrm{gas-phase}}$ and the surface reaction Q_{surf}, is by definition the heat of vaporization of sodium $L_{\mathrm{vap,Na}}$ (eq. (2)). For both surface and gas-phase reactions, the net energy balance is thus $Q = 142\,\mathrm{kJ\,mol^{-1}}$ [21].

$$Q = \underbrace{Q_{\mathrm{gas-phase}} - L_{\mathrm{vap,Na}}}_{Q_{\mathrm{surf}}} - L_{\mathrm{vap,H_2O}} \tag{2}$$

- **Kinetics.** As for many combustion processes, SWR rate is controlled by mixing kinetics of the reactants more than chemical kinetics, which is much faster. As pointed out by Takata et al. [17], SWR is a diffusion-driven process. In this paper, the reaction is considered instantaneous, as it is the case in most SWR models [11, 17].

3.1.3 Interfaces temperature and concentrations

The two interfaces (sodium-gas and gas-water) are considered at thermodynamic equilibrium. It means that thermodynamic equilibrium is reached faster than other kinetics processes. This hypothesis is common in droplet vaporization models, such as Abramzon and Sirignano [22] or Furfaro and Saurel [23] and widely used in spray combustion. Therefore, at an interface between a non-condensable gas g and a liquid l (such as $l = \mathrm{H_2O, Na}$), the vapor molar fraction at the interface is $x^l_{vap} = \frac{P^l_{sat}(T_I)}{P}$ where T_I is the interface temperature and P the absolute pressure. The interface temperature is estimated

from both heat flux and temperature continuity as:

$$T_I = \frac{\lambda_g T_g + \lambda_l T_l}{\lambda_g + \lambda_l}$$

where T is the temperature, λ the thermal conductivity. As for both species and especially sodium, $\lambda_l \gg \lambda_g$, it will be assumed that $T_I \approx T_l$.

3.1.4 Other assumptions

Experimental images show that the film thickness e is roughly constant before the explosion. This is a consequence of equilibrium between gas generation by SWR and loss. Some gas leaves the film to form bubbles or escape into the atmosphere (Fig. 2b, 2c). Experimental images show that $e \approx 1\,\mathrm{mm}$.

Also, as only diffusion flows in the radial direction play a role, and convective gas flows are in the orthoradial direction, the film will be treated as static.

As the latent heat of sodium fusion is negligible compared to its heat of vaporization ($2.6\,\mathrm{kJ\,mol^{-1}}$ *vs.* $97\,\mathrm{kJ\,mol^{-1}}$), and as in experiments sodium fusion always occurs well before runaway and does not seem to be correlated to its onset, no difference is made in the model between solid and liquid sodium.

Last, let us estimate the mass variation of the sodium pellet Δm. It is evaluated as the sodium mass consumed by SWR to heat up sodium from T_0 to T_f:

$$\Delta m = \frac{m_0 c_p (T_f - T_0) M_{\mathrm{Na}}}{Q}$$

with $m_0 = 1\,\mathrm{g}$ the sodium initial mass, c_p its mass heat capacity, and M_{Na} its molar mass. For $T_f = T_b = 883\,^\circ\mathrm{C}$, $\Delta m = 0.19\,\mathrm{g}$. Sodium mass variation is about 20%, which corresponds to a ball radius variation of 7%. This variation is neglected in the following for simplicity.

3.1.5 Summary

The simplifying assumptions made from the previous considerations are summarized hereafter:

- Water temperature is constant ;
- Sodium temperature is uniform and time-varying ;
- SWR takes place at a front distant of e_f from the sodium, is instantaneous and yields a net energy $Q = 142\,\mathrm{kJ\,mol^{-1}}$;
- Interfaces are at liquid temperatures and at saturation ;
- The gas film is treated as static with constant thickness e ;

- Sodium mass variation is neglected during the experiment.

The physical constants and parameters used are given in Table 2.

Table 2: Model constants

Name	Value	Definition
m_0	$1\,\mathrm{g}$	sodium initial mass
e	$1\,\mathrm{mm}$	film thickness
c_p	$1300\,\mathrm{J\,kg^{-1}\,K^{-1}}$	sodium massive heat capacity
R_{Na}	$6.5\,\mathrm{mm}$	sodium pellet radius
Q	$142\,\mathrm{kJ\,mol^{-1}}$	SWR net energy balance
D	$1.3 \times 10^{-4}\,\mathrm{m^2\,s^{-1}}$	molecular diffusion coefficient in the gas film

3.2 Model equations and resolution

3.2.1 Equations

Water and sodium diffusion fluxes in the film are given by Fick's law:

$$\phi_{\mathrm{H_2O}} = -D\frac{\partial c_{\mathrm{H_2O}}}{\partial r} \qquad \phi_{\mathrm{Na}} = -D\frac{\partial c_{\mathrm{Na}}}{\partial r}$$

D is the molecular diffusion coefficient (the same for both species), and c refers to molar concentrations. Given the small thickness of the film, and knowing that concentrations are saturated at interfaces and zero at the reaction front, these relations can be approximated as:

$$\phi_{\mathrm{H_2O}}(t) = -D\frac{c_{sat,\mathrm{H_2O}}(T_{\mathrm{H_2O}})}{e - e_f(t)} \tag{3}$$

$$\phi_{\mathrm{Na}}(t) = D\frac{c_{sat,\mathrm{Na}}(T_{\mathrm{Na}}(t))}{e_f(t)} \tag{4}$$

Energy balance for the sodium pellet reads,

$$\frac{\mathrm{dT_{Na}(t)}}{\mathrm{dt}} = \frac{P(t)}{C} \tag{5}$$

where P is the net thermal power released by the reaction and $C = mc_p$ the sodium sample heat capacity. Now the ideal gas equation of state gives interface concentrations as a function of interface temperatures:

$$c_{sat,\mathrm{H_2O}} = \frac{P_{sat,\mathrm{H_2O}}(T_{\mathrm{H_2O}})}{RT_{\mathrm{H_2O}}} \tag{6}$$

$$c_{sat,\mathrm{Na}}(t) = \frac{P_{sat,\mathrm{Na}}(T_{\mathrm{Na}}(t))}{RT_{\mathrm{Na}}(t)} \tag{7}$$

Water and sodium vapor pressure are known data [20], given in Pascal by:

$$P_{sat,\mathrm{H_2O}}(T_{\mathrm{H_2O}}) = P_0 \exp\left[\frac{L_{vap,\mathrm{H_2O}} M_{\mathrm{H_2O}}}{R}\left(\frac{1}{T_0} - \frac{1}{T_{\mathrm{H_2O}}}\right)\right] \tag{8}$$

$$P_{sat,\mathrm{Na}}(T_{\mathrm{Na}}) = 10^6 \exp\left(a_0 - \frac{b_0}{T_{\mathrm{Na}}} - c_0 \ln(T_{\mathrm{Na}})\right) \tag{9}$$

with $P_0 = 1.013 \times 10^5\,\mathrm{Pa}$, $T_0 = 373.15\,\mathrm{K}$, $M_{\mathrm{H_2O}} = 18.0\,\mathrm{g\,mol^{-1}}$, $L_{vap,\mathrm{H_2O}} = 2257\,\mathrm{kJ\,kg^{-1}}$, $R = 8.314\,\mathrm{J\,K^{-1}\,mol^{-1}}$, $a_0 = 11.9463$, $b_0 = 12633.73$, $c_0 = 0.4672$.

3.2.2 Resolution

The reaction stoichiometry imposes the molar fluxes to balance at the flame surface:

$$\phi_{\mathrm{H_2O}}(t) + \phi_{\mathrm{Na}}(t) = 0$$

which using approximations (3) and (4) determines the flame position:

$$e_f(t) = \frac{e}{1 + \frac{c_{sat,\mathrm{H_2O}}}{c_{sat,\mathrm{Na}}(T_{\mathrm{Na}}(t))}}$$

Injecting the expression of e_f in Equation (4), and multiplying by the average cross-section S, yields the total molar flux :

$$\Phi(t) = \frac{DS}{e}\left[c_{sat,\mathrm{H_2O}} + c_{sat,\mathrm{Na}}(T_{\mathrm{Na}}(t))\right]$$

with $S \approx 4\pi(R_{\mathrm{Na}} + \frac{e}{2})^2$ the film cross-section surface. The thermal power is therefore:

$$P(t) = Q \cdot \Phi(t)$$

Developing the expressions for P and Φ into Equation (5) finally yields:

$$\frac{\mathrm{dT_{Na}}}{\mathrm{dt}} - K\frac{P_{sat,\mathrm{Na}}(T_{\mathrm{Na}})}{T_{\mathrm{Na}}} = K\frac{P_{sat,\mathrm{H_2O}}(T_{\mathrm{H_2O}})}{T_{\mathrm{H_2O}}} \tag{10}$$

with $K = \frac{QDS}{eCR}$. Equation (10) is a first-order Ordinary Differential Equation (ODE), with unknown T_{Na}, function of t. It is integrated numerically using an ODE solver [24]. All other time variables can then be obtained from $T_{\mathrm{Na}}(t)$.

3.3 Admission of a free parameter

The constant K in ODE (10) is critical as it drives the kinetics of the model. It includes all model parameters of Table 2. It should be noted that there are large uncertainty on some of this parameters, namely:

- The diffusion coefficient D, for which little data is available in the literature. Ramsey and Anderson [25] give $D = 1.3 \times 10^{-4}\,\mathrm{m^2\,s^{-1}}$ specifying that the uncertainty on this value is larger than 50%. Daudin [26] argues that in the context of SWR, D might in fact be up to 10 times larger;
- The efficient reaction area S. As detailed in the experimental section 2, runaway occurs either underwater or at the surface depending on sodium temperature. Therefore, the efficient area is lower than S in some cases;
- The film thickness e, which depends on complex physics and was only evaluated from the videos,
- The sodium mass m_{Na}, included in the heat capacity C. As explained in 3.1.4, the variation of m_{Na} is neglected by assumption.

Given these considerations it is unrealistic to assume that K has a physical value. Therefore an adjustable parameter α is admitted to account for the uncertainties in the parameters and K is replaced by αK. EDO (10) becomes:

$$\frac{\mathrm{dT_{Na}}}{\mathrm{dt}} - \alpha K \frac{P_{sat,\mathrm{Na}}(T_{\mathrm{Na}})}{T_{\mathrm{Na}}} = \alpha K \frac{P_{sat,\mathrm{H_2O}}(T_{\mathrm{H_2O}})}{T_{\mathrm{H_2O}}} \tag{11}$$

Results will first be computed with $\alpha = 1$, then α will be adjusted using data from VIPERE experiements.

3.4 Results

Fig. 8 shows the results obtained by numerical resolution of Equation (11) with $\alpha = 1$ for several variables of interest and for three typical water temperatures. It can be noticed that there are 3 distinct phases in the results presented, which correspond to the steps of the phenomenology proposed in Section 2.5.

There is at first a heating phase, when sodium temperature increases linearly. In the meantime, sodium vapor pressure also increases but from so tiny concentrations that it remains negligible. The generated power is constant and $e_f \approx 0$, meaning that at this stage we are in the presence of a surface reaction. Then, there is a rapid increase of all variables. As vapor concentration becomes significant and the reaction front starts to move across the film ($e_f > 0$), the thermal power increases and sodium heating becomes more intense (gas-phase reaction). At the instant the front reaches the gas-water interface ($e_f \approx e$), sodium temperature diverges towards very high values and thermal power jumps by nearly 3 orders of magnitude. This divergence corresponds to the runaway. Consistently with experimental observations, the model also predicts SWR runaway occurs faster as water temperature is increased.

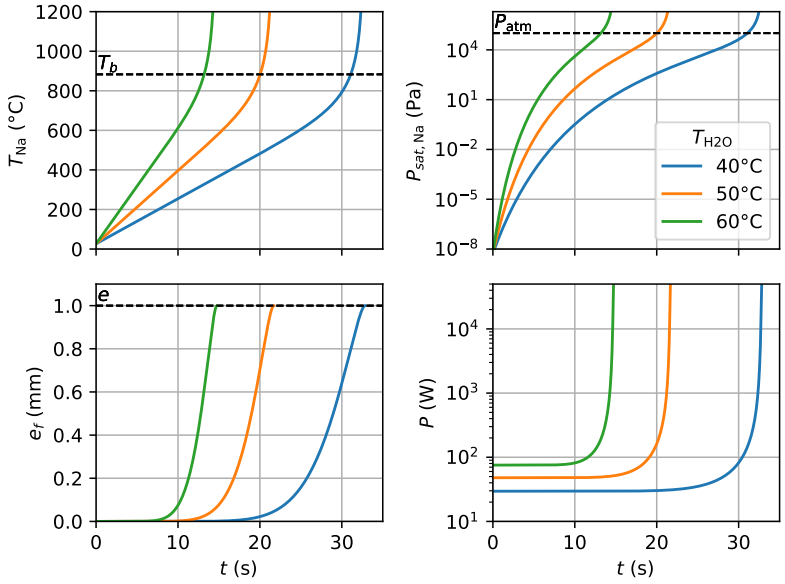

Figure 8: Results obtained by numerical resolution of Equation (11) for different water temperatures with $\alpha = 1$. The behavior of the variables is consistent with experimental observations. The kinetics are slower due to underestimation of α.

We also define the delay time t_d as the time of the abrupt increase of the thermal power P (Fig.9). Numerically, it is computed using a criterion on the power gradient:

$$t_d = \inf \left\{ t \in \mathbb{R}_+ \; ; \; \frac{\mathrm{d}P}{\mathrm{d}t} > 10^5 \, \mathrm{W\,s^{-1}} \right\}$$

The delay time t_d obtained from the model decreases exponentially with water temperature as data measured during VIPERE experiments (Fig. 10). That is because water vapor pressure $P_{sat,\mathrm{H_2O}}$ is an exponential function of $T_{\mathrm{H_2O}}$, thus so is the heating power. With $\alpha = 1$, the delay time is much overestimated compared to experimental values, which is also visible from the slow kinetics in Fig. 8. This means that α is underestimated. With α fitted by the least-squares method using experimental delay times ($\alpha = 8.12$), a solid consistency between the model and the data is obtained.

Similarly to thermal explosions models of Semenov [15] and Kamenetskii [16], that models features a heating phase that eventually triggers a runaway. Apart from extra physics that needed to be added due to the heterogeneous nature of SWR, the main difference is that here the runaway is not triggered by the reaction kinetics (exponential Arrhenius law) but by the vaporization of the reactants (exponential sodium vapor pressure).

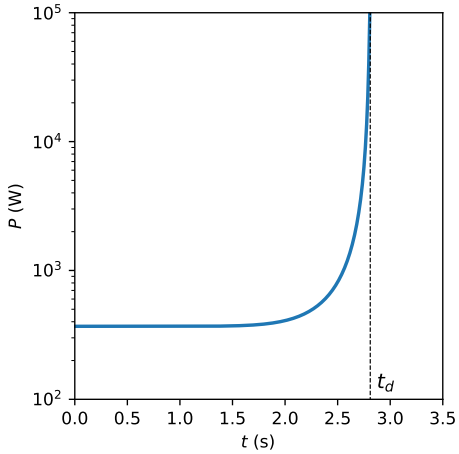

Figure 9: The delay time is numerically defined as the time of the abrupt thermal power increase.

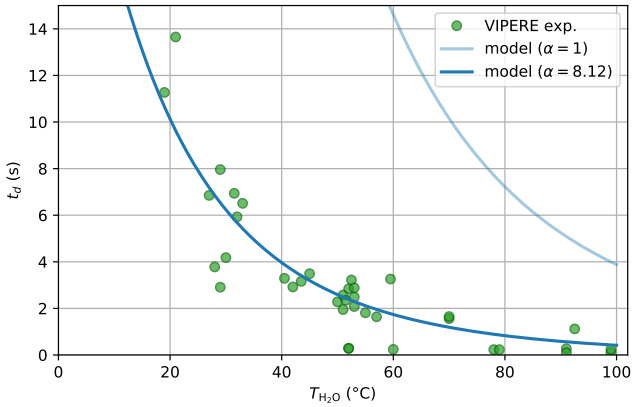

Figure 10: The trend obtained for the delay time is consistent with data from VIPERE experiments. If the parameter α is properly adjusted (by the least square method for example), quantitative agreement is also obtained.

3.5 Model extensions

As shown in Section 3.4, the results from the basic model qualitatively reproduce experimental observations. In this section we propose two extensions: the introduction of a temperature-variable diffusion coefficient and the introduction of a linear heat loss term.

3.5.1 Temperature-variable diffusion coefficient

It is known from kinetic theory of gases that D is not constant with temperature but increases with $T^{3/2}$. Therefore taking a constant value of D leads to an underestimation of diffusion fluxes and can explain why α had to be set to a high value to match experimental data. Accurately accounting for the variations of D with gas temperature is beyond the scope of this model, which does not compute the gas temperature. Still, in first approximation, we can assume that the gas temperature is equal to the sodium temperature T_{Na}. Doing the same resolution of Equation (10) with:

$$D(T_{\mathrm{Na}}) = D_0 \left(\frac{T_{\mathrm{Na}}}{T_0} \right)^{\frac{3}{2}}$$

with $D_0 = 1.3 \times 10^{-4}\,\mathrm{m^2\,s^{-1}}$ and $T_0 = 298\,\mathrm{K}$, allows to match experimental delay time values with $\alpha = 3.16$ (Figure 12).

3.5.2 Introduction of a heat loss term

A linear heat loss term can be added to the model as in the Semenov model [15]. This added term extends the model capability with the possibility to predict whether a runaway will occur or not. The introduction of a heat loss term indeed creates a competition between heat production and losses. Depending on the relative magnitude of these two contributions, the results will be either a runaway or a steady-state regime. On the counterpart, this adds another parameter α_2 to adjust. With this new contribution, EDO (11) becomes:

$$\frac{\mathrm{dT_{Na}}}{\mathrm{dt}} - \alpha K \frac{P_{sat,\mathrm{Na}}(T_{\mathrm{Na}})}{T_{\mathrm{Na}}} = \alpha K \frac{P_{sat,\mathrm{H_2O}}(T_{\mathrm{H_2O}})}{T_{\mathrm{H_2O}}} - \alpha_2 \frac{T_{\mathrm{Na}} - T_{\mathrm{H_2O}}}{e^2} \tag{12}$$

As a first guess for α_2, it is set to the value that places the threshold between steady-state and runaway regimes at $T_{\mathrm{H_2O}} = 27\,^{\circ}\mathrm{C}$. This corresponds to the temperature under which there were almost no runaway (2/7 tests) in the experiments. As seen from Fig. 11, steady-state and runaway regimes are reproduced as expected for low water temperatures. Regarding delay times (Fig. 12), results appear to be qualitatively less accurate than for the basic model. However, only the version integrating heat loss gives a correct prediction (no runaway, *i.e.* infinite delay time) for the 5 tests without runaway for $T_{\mathrm{H_2O}} < 27\,^{\circ}\mathrm{C}$.

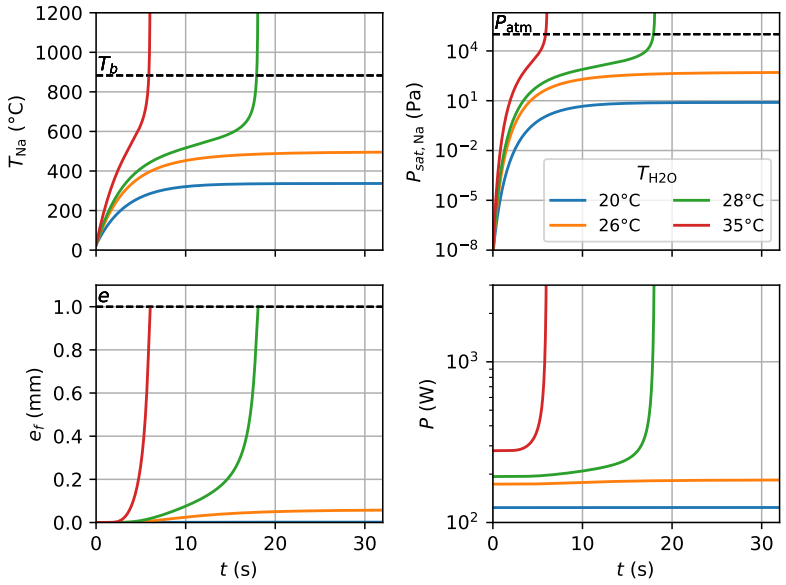

Figure 11: Results with linear heat loss (Equation (12)) for sample water temperatures with $\alpha = 12.2$ and $\alpha_2 = 3.13 \times 10^{-7}\,\mathrm{m^2\,s^{-1}}$. With the introduction of the heat loss term, steady-state regimes are obtained for low water temperatures.

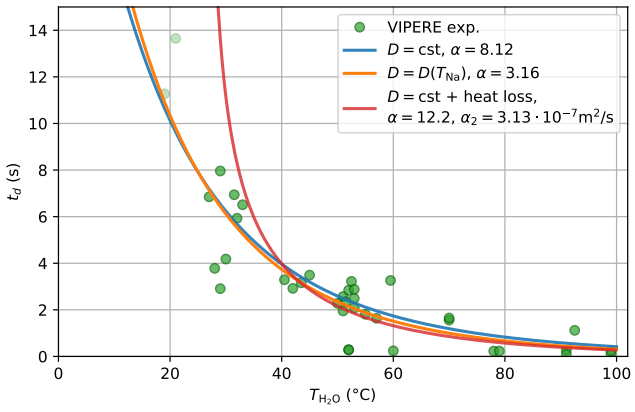

Figure 12: Delay times computed for the basic model, with temperature-variable diffusion coefficient, and with a heat loss term.

Conclusion

Experimental investigation of sodium-water reaction at small scale has been carried out using high-speed imagery. A fume that is believed to be sodium vapor was repeatedly observed in the instants preceding explosions. This information suggests that sodium vaporization is a key element in the still unexplained mechanism of sodium water reaction runaway.

A simplified semi-analytic model close to thermal explosion models has been developed to describe the dynamics of sodium heating and diffusion processes through the gas film separating reactants. Its predictions are qualitatively consistent with experimental observations, and even quantitatively if the parameter α is set to an optimized value, which proves to be realistic. The model can also be extended to steady-state cases if a second parameter is added, enabling to predict whether a runaway will occur or not. Modeling results also demonstrate the role of sodium vaporization in the triggering of SWR runaway.

Future work is needed to validate that hypothesis and to extend the modeling capabilities towards a prediction of SWR effects, in particular the quantity of sodium reacting at once during runaways and pressure effects. The preparation of a new experiment involving optical measurements of sodium vapor concentration, as well as the development of a SWR numerical simulation code, are underway in that purpose.

Funding

This work was supported by the French Atomic Energy and Alternative Energies Commission (CEA).

References

[1] Takashi Takata, Akira Yamaguchi, Akihiro Uchibori, and Hiroyuki Ohshima. Computational methodology of sodium-water reaction phenomenon in steam generator of sodium-cooled fast reactor. *Journal of nuclear science and technology*, 46(6):613–623, 2009.

[2] Francis Roger, Jean-Louis Carreau, Laurent Gbahoué, Philippe Hobbes, Alexandre Allou, and François Beauchamp. Structure of strongly underexpanded gas jets submerged in liquids–application to the wastage of tubes by aggressive jets. *Nuclear Engineering and Design*, 273: 119–130, 2014.

[3] Sergey Perevoznikov, Yuriy Shvetsov, Aleksey Kamayev, Ilia Pakhomov, Viacheslav Borisov, Gennadiy Pazin, Oleg Mirzeabasov, and Olga Korzun. Modeling of hydrodynamic processes at a large leak of water into sodium in the fast reactor coolant circuit. *Nuclear Engineering and Technology*, 48(5):1162–1173, 2016.

[4] Belikov VV, Vasilev SI, Veretentsev VA, Kolobaeva PV, Mosunova NA, Usov EV, and VV Chudanov. Modeling of liquid metal flow using system thermohydraulic code HYDRA-IBRAE/LM and CFD code CONV-3D.

[5] C.C. Addison. *The chemistry of the liquid alkali metals*. John Wiley and Sons, Inc., New York, NY, 1984.

[6] S. Carnevali, C. Proust, and M. Soucille. Unsteady aspects of sodium–water–air reaction. *Chemical Engineering Research and Design*, 91(4):633–639, 2013.

[7] S. Carnevali. *Unsteady aspects of sodium-water reaction : water cleaning of sodium containing equipments*. PhD thesis, Génie des Procédś Industriels et dv́eloppement durable, UTC Compiègne, 2012.

[8] K. Daudin, F. Beauchamp, and C. Proust. Phenomenological study of the pre-mixing step of sodium-water explosive interaction. *Experimental Thermal and Fluid Science*, 91:1–8, 2017.

[9] A.B. Ashworth. *Reactions between the liquid alkali-metals and liquid water*. PhD thesis, University of Nottingham, 1979.

[10] Ph.E. Mason, F. Uhlig, V. Vaněk, T. Buttersack, S. Bauerecker, and P. Jungwirth. Coulomb explosion during the early stages of the reaction of alkali metals with water. *Nature chemistry*, 7 (3):250–254, 2015.

[11] O. Marfaing. *Contributions to the fine-scale modeling of sodium-water reaction*. PhD thesis, UPMC, CEA, 2014.

[12] M. Bader and C.A. Busse. Wetting by sodium at high temperatures in pure vapour atmosphere. *Journal of Nuclear Materials*, 67(3):295–300, 1977.

[13] Ph.E. Mason, T. Buttersack, S. Bauerecker, and P. Jungwirth. A non-exploding alkali metal drop on water: From blue solvated electrons to bursting molten hydroxide. *Angewandte Chemie International Edition*, 55(42):13019–13022, 2016.

[14] J.J. de Groot, J. Schlejen, and J.P. Woerdman. The influence of NaNa, NaHg and NaXe molecules on the spectrum of the high-pressure sodium lamp. *Philips J. Res*, 42:87–101, 1987.

[15] N.N. Semenov. The calculation of critical temperatures of thermal explosion. *Z Phys Chem*, 48: 571, 1928.

[16] D. A. Frank-Kamenetskii and N. Thon. *Diffusion and Heat Exchange in Chemical Kinetics*. Princeton University Press, 1955. ISBN 9780691626932.

[17] T. Takata, A. Yamaguchi, K. Fukuzawa, and K. Matsubara. Numerical methodology of sodium-water reaction with multiphase flow analysis. *Nuclear Science and Engineering*, 150(2):221–236, 2005.

[18] M.L. Corradini, B.J. Kim, and M.D. Oh. Vapor explosions in light water reactors: a review of theory and modeling. *Progress in Nuclear Energy*, 22(1):1–117, 1988.

[19] C.H. Wang, X.Q. Liu, and C.K. Law. Combustion and microexplosion of freely falling multicomponent droplets. *Combustion and Flame*, 56(2):175 – 197, 1984. doi: https://doi.org/10.1016/0010-2180(84)90036-1.

[20] J.K. Fink and L. Leibowitz. Thermodynamic and transport properties of sodium liquid and vapor. Technical report, Argonne National Lab., IL (United States), 1995.

[21] M.W. Chase. NIST-JANAF thermochemical tables. *Journal of Physical and Chemical Reference Data*, 25(2):551–603, 1996.

[22] B. Abramzon and W.A. Sirignano. Droplet vaporization model for spray combustion calculations. *International Journal of Heat and Mass Transfer*, 32(9):1605–1618, 1989.

[23] D. Furfaro and R. Saurel. Modeling droplet phase change in the presence of a multi-component gas mixture. *Applied Mathematics and Computation*, 272:518–541, 2016.

[24] E. Jones, T. Oliphant, P. Peterson, et al. SciPy: Open source scientific tools for Python, 2001–. URL `http://www.scipy.org/`. [Online; accessed 07-12-2018].

[25] A.T. Ramsey and L.W. Anderson. Spin relaxation in an optically oriented sodium vapor. *Il Nuovo Cimento (1955-1965)*, 32(5):1151–1157, 1964.

[26] Kevin Daudin. *Contribution ÃÂ la prédiction des effets des réactions sodium-eau: application aux pertes de confinement dans un bâtiment générateur de vapeur d'un réacteur à neutrons rapides refroidi au sodium.* PhD thesis, UTC-CEA, 2015.